coatings

MDPI

Article

Effect of Spraying Power on the Tribological Properties of Alumina and Alumina-Graphite Coatings

Jacob Shiby Mathew [1], Liutauras Marcinauskas [1,2,*], Žydrūnas Kavaliauskas [2], Romualdas Kėželis [2] and Mitjan Kalin [3]

[1] Department of Physics, Kaunas University of Technology, Studentu Str. 50, LT-51368 Kaunas, Lithuania; jacob.mathew@ktu.lt
[2] Plasma Processing Laboratory, Lithuanian Energy Institute, Breslaujos Str. 3, LT-44403 Kaunas, Lithuania; zydrunas.kavaliauskas@lei.lt (Ž.K.); romualdas.kezelis@lei.lt (R.K.)
[3] Laboratory for Tribology and Interface Nanotechnology, Faculty of Mechanical Engineering, University of Ljubljana, Bogišićeva 8, 1000 Ljubljana, Slovenia; mitjan.kalin@fs.uni-lj.si
* Correspondence: liutauras.marcinauskas@ktu.lt

Abstract: Atmospheric plasma spraying is used to deposit alumina and alumina-graphite composite coatings. The influence of arc current (plasma temperature) on the microstructure, roughness, elemental composition, and phase composition of the coatings is analyzed by scanning electron microscopy (SEM), surface roughness testing, energy dispersive X-ray spectroscopy (EDX), and X-ray diffraction (XRD). The tribological properties of the sprayed coatings are analyzed using a tribometer with a ball-on-flat configuration. The roughness of the as-sprayed coatings increases and the size of the granules decreases with the increase in plasma temperature. The results demonstrate that the friction coefficients and wear rates are slightly reduced for Al_2O_3 coatings sprayed at higher arc currents. The Al_2O_3-graphite coatings register lower friction coefficient values than the Al_2O_3 coatings under dry sliding conditions.

Keywords: alumina-graphite coatings; plasma spraying; tribology; friction coefficient

Citation: Mathew, J.S.; Marcinauskas, L.; Kavaliauskas, Ž.; Kėželis, R.; Kalin, M. Effect of Spraying Power on the Tribological Properties of Alumina and Alumina-Graphite Coatings. *Coatings* **2023**, *13*, 1165. https://doi.org/10.3390/coatings13071165

Academic Editor: Dimitrios Tasis

Received: 11 May 2023
Revised: 21 June 2023
Accepted: 22 June 2023
Published: 27 June 2023

1. Introduction

Plasma spraying is a multifaceted process that can potentially be used to coat steel surfaces that suffer much deterioration due to their low intrinsic hardness. The densification of the coating material with an ability to produce thick coatings; a high flame temperature with a competent particle velocity; swiftness and flexibility of the coating process; and cost efficiency are some of the meritorious aspects of plasma spraying [1–4]. The main advantages of plasma spraying are the high deposition efficiency and desirable characteristics of the as-sprayed coatings. Thermally sprayed coatings are used in the paper industry for the protection of paper machine rolls, doctor blades, dryer drums, or hydraulic valve plungers from wear or corrosion [1,5–7]. It should be mentioned that plasma-sprayed Al_2O_3 and alumina composite coatings are widely used as customary industrial materials due to their high hardness, proper strength and toughness, and superior tribological and insulation characteristics [8–12]. In a sense, the properties of the alumina and alumina composite coatings can be controlled by the addition of filler materials, post-treatment processes, and initial feedstock powder characteristics, but an imperative factor is also the adjustment of plasma spraying parameters such as torch power, gas flow rate, and deposition distance [13–17]. The latter has a direct impact on the mechanical and tribological properties of the coatings in relation to the high hardness of the ceramic alumina [1,18].

R. Wang et al. demonstrated that with the increase in torch power from 25 to 45 kW, the melting degree of particles and the bonding strength increased for Zn-Al coatings

from 8.2 to 13.8 MPa, with 40 kW being the most favorable power [19]. H. Wu et al. showed that for $MoSi_2$ coatings, with an increase in torch power from 40 to 55 kW, the coatings had become more compact with a proliferation of bonding strength. The coating produced at 50 kW was most competent, with a bonding strength of 14.5 MPa [20]. J. Wang et al. demonstrated that for nanostructured yttria-stabilized zirconia coatings, out of torch powers ranging from 22 to 45 kW, the coatings deposited at 22 kW showed a stable-phase structure and the required thermal shock resistance. The correspondingly achieved bonding strength of 29 MPa and the thermal cycling life of 292 cycles were found to be approximately twice higher than the highest bond-coat spraying power [21]. C. Wang et al. [22] studied the effect of spraying powers ranging from 45 to 60 kW on La-doped Mo-Si ceramic coatings and found that with an increase in power, the feedstock particle compactness increased. They had also discovered that the torch power at 55 kW was the most remarkable, with a distinguished oxidation resistance as seen in the coating and a low mass loss to the tune of 1.18% [22]. X. C. Zhang et al. [23] demonstrated that with an increase in torch power from 43.2 up to 57 kW, the number of unmelted particles decreased. It was also observed that with the increase in power, the porosity decreased while the Young's modulus and microhardness of coatings increased. It must also be mentioned that with increasing Young's modulus, enhancement of the residual stress was observed [23]. Y. Z. Xing et al. showed that for cast-iron coatings deposited using torch powers ranging from 15 to 30 kW, the splat-substrate adhesion increased with an increase in torch power. This was mainly attributed to elevated temperatures and particle velocities promoting the heating effect at the substrate surface for better coating characteristics [24]. C. Wang et al. [15] had prepared Al_2O_3 coatings at power ranging from 52 to 60 kW and found that with an increase in power for the range from 52 to 58 kW, the compactness, Vicker's strength, and flexural strength had increased, whereas in the final range of 60 kW there was an opposite trend due to crack formation. D. Zhao et al. [25] showed that with an increase in torch power from 98 to 145 kW (at a short spraying distance), the hardness of coatings increased and porosity decreased due to better melting of feedstock powders. Meanwhile, decreasing the torch power with an increase in spraying distance caused the re-solidification of particles and unmelted powder. G. Sivakumar et al. [26] expressed that continuous exposure of the in-flight particles to the plasma plume at torch powers of 35 and 46 kW was synonymous with a heat treatment process with the formation of pure alpha-phase alumina coatings. R. G. Song et al. [27] demonstrated for Al_2O_3/TiO_2 coatings that with an increase in spraying power from 20 kW to 35 kW, the gamma-Al_2O_3 phase increased substantially, consisting of bi-modal structures. The amount of partially melted fragments decreased with an increase in torch power, giving rise to a completely melted lamellar structure. The microhardness and wear resistance had a mixed trend, increasing initially and then dropping with increasing torch power. C. J. Luhad [28] showed that for low torch powers in the range from 2.2–3.9 kW, a feasible coating could still be produced if the particle velocity and the molten state were competently achieved. It was shown that even with low torch powers, a particle molten state was achieved prior to deposition, thereby defining good surface characteristics. Similarly, alumina coatings prepared by Y. Gao et al. [29] with low torch powers in the range from 2.5 to 4 kW depicted that with increasing torch power on an internally fed setup, the hardness increased and consisted of phase gamma-alumina against the initially near-complete alpha-alumina phase, which had decreased in the coatings. E.P. Song et al. [16] showed that with increasing torch power based on the critical spray plasma parameter (CPSP), the partially melted regions and the gamma-alumina phase increased while the porosity decreased. Additionally, wear resistance and hardness had also increased. Z. Bu et al. [30] demonstrated that the increase of the spraying power enhanced the particle temperature and velocity. As a result the content of gamma-Al_2O_3 phase was enhanced. G. Bolelli et al. [31] demonstrated that with plasma-sprayed Al_2O_3 coatings, one of the biggest merits was the fact that they did not undergo abrasive grooving but just splat detachments, showing competent abrasive resistance.

The addition of carbon-based materials is an effective way to improve the tribological properties of alumina coatings. It was found that the addition of a low amount of graphene nanoplatelets (up to 3 wt.%) and graphene oxide (GO) enhanced the specific wear rate and reduced the friction coefficient of alumina-graphene composite coatings [32–34]. Our previous investigations [35–37] demonstrated that the friction coefficients and specific wear rates of alumina-graphite coatings are dependent not only on the concentration of graphite in the alumina feedstock powder but also on the type of Al_2O_3 and graphite powders used. It was demonstrated that the increase in spraying distance enhanced the friction coefficient of alumina-graphite coatings from 0.34 to 0.38 [36]. Meanwhile, the variation of the graphite concentration in the feedstock powders allowed for manipulation of the friction coefficient and wear rate of alumina-graphite coatings [35,37]. Al_2O_3 coatings are generally found to exhibit high wear rates and friction coefficients, but with the addition of a solid lubricant such as graphite, extrinsic modifications can be made. X. Zhao et al. [38] used the solid-lubricant graphite as an additive material in composite coatings. A reasonable amount of graphite in the composite coating retained competent hardness without affecting it negatively. It was observed that using 20 wt.% Ni-graphite reduced the friction coefficient and wear rate of coatings by 52% and 4.15 times, respectively. Thus, Al_2O_3 coatings with a solid lubricant such as graphite produced by plasma spraying are promising for improving the tribological properties and controlling the surface morphology. The information on the formation of aluminum oxide coatings using graphite as an additive material is insufficient. So, it is necessary to determine how the concentration of graphite, size of particles, or torch power affects the structure, elemental concentration, phase composition, mechanical properties, and tribological properties of the plasma sprayed coatings.

The main aims were to investigate the influence of the graphite addition on the microstructure and tribological properties of aluminum oxide coatings and to determine the influence of the plasma temperature on the friction coefficient and wear rate of aluminum oxide - graphite coatings deposited by plasma spraying.

2. Materials and Methods

The coatings were deposited on AISI 304L substrates at atmospheric pressure using a direct current plasma torch. The plasma torch used in this experiment was constructed at the Lithuanian Energy Institute (Kaunas, Lithuania) [39]. The steel substrates (dimensions of 40 mm × 10 mm × 1.5 mm) were polished and chemically cleaned before starting the formation process. The steel substrates were located on a water-cooled sample holder. Air was used as both the primary gas (total flow rate of 4.72 g/s) and the powder carrier gas (flow rate of 0.60 g/s). Hydrogen (0.1 g/s) was used as the secondary gas to increase the plasma temperature. The deposition was done using a cylindrically shaped length of 150 mm reactor that was connected to the exit of the plasma torch anode.

The Al_2O_3 (A) and Al_2O_3-10 wt.% graphite (AG) powders were used as feedstock materials. Sprayed alumina powders were of a non-regular shape with a size range from 63 to 140 μm [40]. The size of the graphite powders was in the range of 20–63 μm. The images of used feedstock powders are given in ref. 41. The feedstock powders were dried for 18 h at ~330 K before starting the spraying process. The powders were injected into the reactor nozzle at a distance of 150 mm from the exit. The plasma torch was moving in the *x*-axis direction both forward and backward (1 pass) during the spraying. Coatings were deposited with a torch moving perpendicularly to the substrate, and seven passes were made. The spraying distance was 70 mm, and the duration was 40 s. The coatings were deposited at various arc currents (Table 1). Each coating-series had a set of several coatings to ensure a feasible repeatability factor.

The mean plasma temperature in the injection place of the powders and the average plasma temperature and velocity at the nozzle outlet were calculated from the heat balance corresponding to the plasma enthalpy as given in Table 1. The detailed methodology of the plasma velocity and temperature calculations is presented in ref. [41].

Table 1. The deposition parameters of the coatings.

Parameter	Al_2O_3	Al_2O_3	Al_2O_3	Al_2O_3-Graphite	Al_2O_3-Graphite	Al_2O_3-Graphite
Coating	A1	A2	A3	AG1	AG2	AG3
Current, A	180	200	220	180	200	220
Voltage, V	205	202	195	202	198	192
Power, kW	36.9	40.4	42.9	36.36	39.6	42.24
Spray distance, mm	70	70	70	70	70	70
Temperature, K	3400 ± 50	3445 ± 50	3485 ± 50	3380 ± 50	3450 ± 50	3480 ± 50
Velocity, m/s	1350 ± 20	1370 ± 20	1385 ± 20	1340 ± 20	1365 ± 20	1380 ± 20

The morphology of the Al_2O_3 and Al_2O_3-graphite coatings was investigated by scanning electron microscopy (SEM) using a Hitachi S-3400N (Tokyo, Japan). The elemental composition was determined by energy dispersive X-ray spectroscopy (EDX) (Bruker Quad 5040 spectrometer, Hamburg, Germany). The measurements were performed at 5 different points (surface area of 1.05 mm^2). The surface roughness of the coatings was measured on a portable surface roughness tester, Mitutoyo Surftest SJ-210 Series (Version 2.00 with standard ISO 1997). Roughness was measured with a standard surface indenter, and for relevant statistical evaluation, the measurements on each coating were carried out at least 4 times, the length of one measurement was 4 mm. The phase composition was measured by X-ray diffraction (XRD) (Bruker D8 Discover, Billerica, MA, USA) with a standard Bragg–Brentano focusing geometry in a 5°–80° range using the CuKα (λ = 0.154059 nm) radiation. The tribological tests were done on a tribometer (UMT-2, CETR, Campbell, CA, USA) using a ball-on-flat configuration. The upper specimen was an Al_2O_3 ball (purity 99.5%, grade 10, and diameter 10 mm), and the lower specimens were Al_2O_3 or Al_2O_3-graphite coatings deposited on stainless steel. The tests were performed using a constant normal load of 0.8 N with a frequency of 10 Hz and a sliding velocity of 0.05 m/s for 3000 s. The stroke length was 5 mm, and the overall sliding distance was 150 m. The sliding tests were carried out under dry-sliding conditions (without additional lubrication) at 21 °C and relative humidity RH = 20 ± 5%. Additional details can be found in [36]. The average friction coefficient was determined by taking the data of the last 10% (sliding time from 2700 to 3000 s) and calculating the average value. After the sliding test, the amount of material removed from the coatings was analyzed with a 3D white-light optical interferometer (Counter GT-K0, Bruker, Billerica, MA, USA), with the use of software Vision64. The normalized wear rates of coatings were calculated from the depth profiles of wear scars using the standard procedure [36].

3. Results

The surface morphology of the as-sprayed alumina and alumina-graphite coatings under various torch powers is shown in Figures 1 and 2. From the SEM images, it could be observed that for alumina coatings with an increase in torch power, the percentage of the molten particles increased and the compactness of the coatings slightly improved toward the highest torch power (Figure 1). The shape of the particles observed on the surface was changing from irregular to spheric-like. The particle size varied between 1 and 10 μm for alumina coatings (Figure 1b,d).

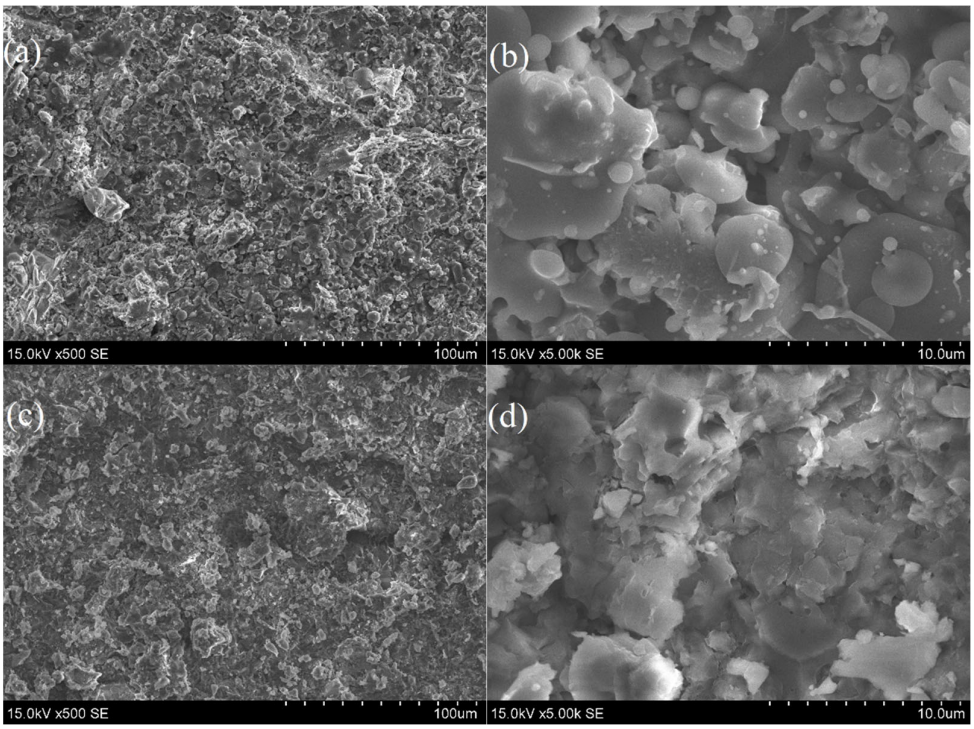

Figure 1. Surface morphology images of (**a**–**d**) Al_2O_3 coatings sprayed at (**a**,**c**) the lowest and (**b**,**d**) the highest torch powers.

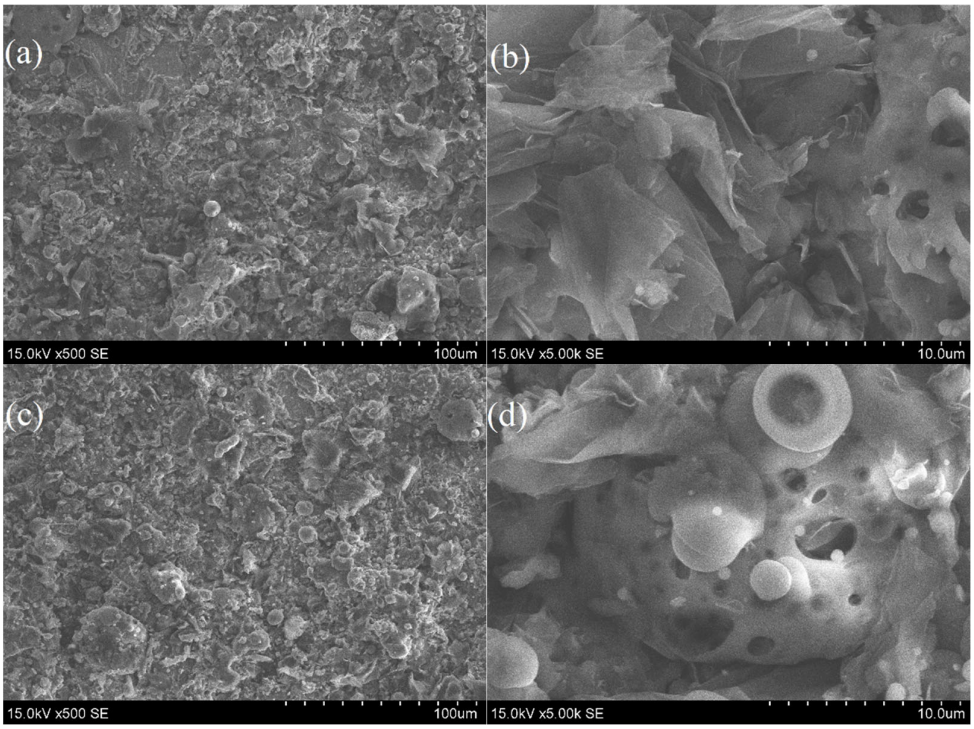

Figure 2. Surface morphology views of Al_2O_3-graphite coatings deposited at (**a**,**b**) the lowest and (**c**,**d**) the highest torch powers.

In the case of alumina-graphite coatings, the presence of semi-melted particles in the form of globules and flakes could be observed (Figure 2). With the increase in torch power, the globular size increased and then seemingly normalized at the highest torch power

(Figure 2d). The particle size varied from 2–20 μm; however, randomly distributed higher-sized particles could be found. The presence of interfacial voids was noticed.

In order to determine the distribution of graphite in the aluminum oxide coatings, EDS mapping was performed. The distribution of aluminum, oxygen, and graphite on the surface of coating (AG2) deposited at 200 A current is given in Figure 3. The surface images of the composite coating deposited at 39.6 kW power indicated that the graphite particles were spread quite homogeneously and were present on the entire surface (Figure 3c). It should be noted that the size of the graphite particles varied from 10 to 40 μm. A similar distribution of the graphite was observed for other Al_2O_3-graphite coatings. Within alumina coatings, the normalized weight percentage ratio of oxygen to aluminum (O/Al) had only changed marginally, taking values in the range of 1.00 to 0.97 from the lowest to the highest torch power. The spread was observed to be increasingly homogeneous with torch power.

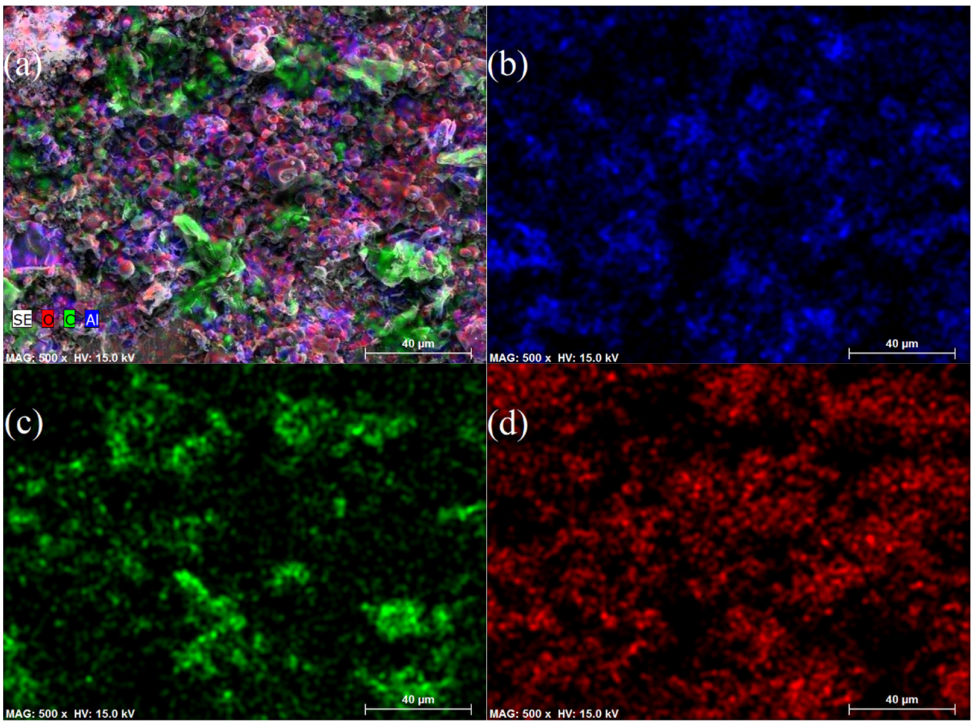

Figure 3. EDS elemental mapping of Al_2O_3-graphite coating formed at (**a**) 39.6 kW, (**b**) aluminum, (**c**) graphite, and (**d**) oxygen.

In the case of alumina-graphite coatings, the oxygen and aluminum contents were reduced with the incorporation of carbon. It was observed that the O/Al ratio had first increased and then decreased, with torch power increasing, depicting values of 1.65, 1.80, and 1.70. The major elements herein were carbon, oxygen, and aluminum. The highest concentration of oxygen was observed in the coatings deposited at the highest torch power. It was observed that the graphite content in the coatings was ~30 wt.%, 27 wt.%, and 26 wt.% for torch powers of ~36.4 kW, 39.6 kW, and ~42.2 kW, respectively. Thus, the graphite weight percentage upon spraying was increased more than twice compared to the initial feedstock powder. The O/C mass ratio increased from 1.10 to 1.38 and up to 1.42 with the increase in torch power. The increase in the oxygen/carbon ratio indicates a higher fraction of oxygen in the coatings. The highest content of oxygen obtained at the highest torch power could be a result of enhanced oxidation of graphite particles in the plasma jet due to increased plasma temperature during deposition. There was a noticeable weight percentage of silicon, yielding 6–7 wt.%.

The variation of surface roughness with respect to arc currents for the coatings, is given in Figure 4. With an increase in arc current, it could be seen that the surface roughness (R_a) for alumina coatings had increased from 3.79 to 4.56 μm. Whereas in the case of alumina-graphite coatings, the average surface roughness range was from 3.17 to 3.44 μm (Figure 4). With the addition of graphite within every torch power scheme, it could be observed that the surface roughness had significantly decreased, from 3.79 to 3.17 μm, from 4.04 to 3.41 μm and from 4.56 to 3.44 μm for ~36 kW, ~40 kW, and ~42 kW, respectively. Similar variational trends were observed for the root mean square roughness (R_q) values of the coatings. The reasons could be attributed to the self-lubricating properties of graphite and its relatively smaller size in comparison to alumina within the feedstock powders.

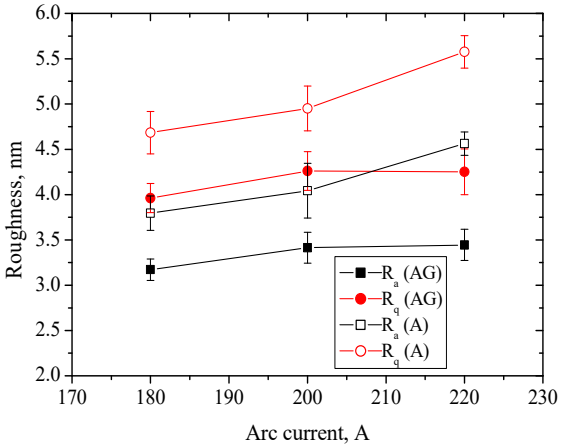

Figure 4. Surface roughness of alumina (A) and alumina–graphite (AG) coatings.

XRD patterns of deposited Al_2O_3 and Al_2O_3-graphite coatings at various torch powers are presented in Figure 5. There was a significant difference in the intensities of the peaks of Al_2O_3 coatings with variations in torch power. It should be noted that Al_2O_3 coatings consisted of rhombohedral α-Al_2O_3, hexagonal β-Al_2O_3, and cubic γ-Al_2O_3 phases. Additionally, it was determined that β-Al_2O_3 is the main phase of the as-sprayed Al_2O_3 coatings (Figure 5a). The high and low intensity peaks at ~7.8° and ~15.7° are associated with sodium aluminum oxide (card No. 32-1033) with the β-alumina (002) and (004) orientations, respectively. The low intensity peak at ~33.2° was attributed to β-Al_2O_3 phase [36]. The highest intensity peak obtained at ~43.7° could be attributed to α-Al_2O_3 (113) phase in addition to signals from the steel substrate. α-Al_2O_3 phase with crystallographic orientations (012) at 25.7°, (104) at 35.2°, and (116) at 57.6° were also observed in the coatings (card No. 83-2080). The low-intensity peaks at 45.9° and 66.9° are attributed to γ-Al_2O_3 phases in alumina coatings (card No. 75-921) [15,21,32,36]. In order to determine structural changes in the alumina coatings, the intensity ratio of the highest peaks attributed to α (35.2°), γ (45.9°), and β (7.8°) phases was determined. The β-Al_2O_3/γ-Al_2O_3 and α-Al_2O_3/γ-Al_2O_3 ratios were reduced from 6.0 to 5.9 and from 2.0 to 1.6 with the increase in troch power, respectively. The β-Al_2O_3/α-Al_2O_3 ratio was enhanced from ~3.1 to ~3.6. Those results indicated that the amount of gamma phase was enhanced and the alpha phase was reduced in the alumina coatings with the torch power increase.

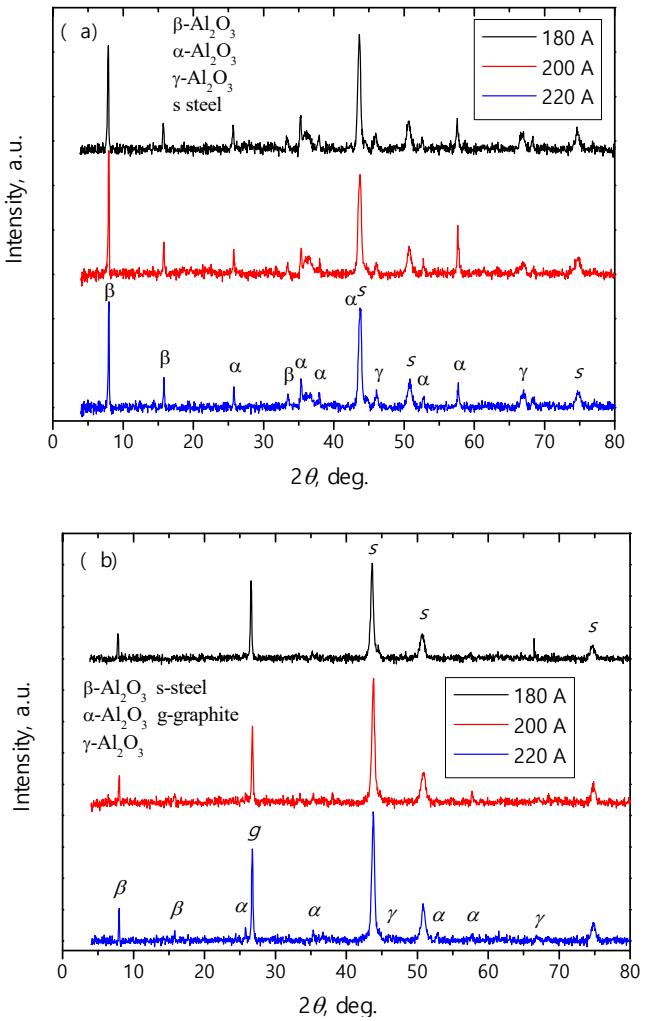

Figure 5. XRD patterns of as-sprayed (**a**) alumina and (**b**) alumina-graphite coatings.

With the addition of graphite to feedstock powders (Figure 5b), changes in the XRD patterns of the as-sprayed Al_2O_3-graphite coatings were noted. The additional narrow peak at 2θ = 26.6° was found and was attributed to the formation of crystalline graphite (002) in the coatings. The intensities of the alumina peaks were reduced with graphite incorporation for all used arc currents (Figure 5b). The intensities of the graphite, β-Al_2O_3 and γ-Al_2O_3 peaks slightly increased with the increase in arc current from 180 A to 220 A. In order to determine the changes in the phase composition of Al_2O_3-graphite coatings, the intensity ratios of peaks were calculated. The β-Al_2O_3/γ-Al_2O_3 ratio was reduced from 5.9 to 4.8 with the increase in torch power. The graphite/β-Al_2O_3 ratio changed from 3.13 to 2.82, while the graphite/γ-Al_2O_3 ratio was reduced from 18.5 to 13.7 with the increase in torch power. These results indicate that the fraction of gamma alumina in the coatings was slightly enhanced with the increase in torch power. It is a well-known fact that the fraction of γ-Al_2O_3 phase in the alumina coatings increases with the increase in melting degree of the feedstock particles. Also, a sufficient cooling of the substrate must be ensured in order to obtain a higher amount of γ-Al_2O_3 phase from the melted state [15,21,28, 30]. J.T. Kim et al. [42] observed that the increase in plasma temperature increased the intensities of β- and β″-alumina peaks in the coatings. C.J. Li et al. [28] found that the gamma-phase content increased and the abrasive wear loss for the Al_2O_3 coatings decreased significantly with an increase in plasma power. Y. Li et al. [34] demonstrated that the addition of GO to alumina coatings enhanced the γ-Al_2O_3 phase content. The increase

in fraction of the γ-Al_2O_3 phase was attributed to the higher thermal conductivity of the GO particles. Thus, the thermal conductivity of graphite is also higher compared to alumina, which could promote better adhesion between the individual alumina lamellas in the coatings. T. Ghara et al. [43] indicated that the increase in arc current from 400 to 450 A resulted in an increase in the average Al_2O_3 particle temperature from 2590 up to 2624 °C. As a result, the gamma phase content was slightly enhanced in the coatings. The increase in torch power (arc current) increased the plasma temperature by 100 degrees (Table 1). Thus, more heat was transferred to the particles; the melting degree of the alumina feedstock powders increased; and this resulted in an insignificant enhancement in the β-Al_2O_3 and γ-Al_2O_3 phase fractions in the formed coatings [15,28,30,43].

The dependence of friction coefficient vs. sliding time for the Al_2O_3 coatings is shown in Figure 6a. The friction coefficient of the as-sprayed Al_2O_3 coatings increased with sliding time, reaching steady-state values of ~0.7 after 400–500 s. When the steady state was reached, the friction coefficients of the alumina coatings deposited at different torch powers were relatively stable with minor fluctuating peaks. The average friction coefficient for the arc currents was evaluated (Figure 7). The friction coefficient of alumina coatings seemed to steadily decrease with the increase in torch power.

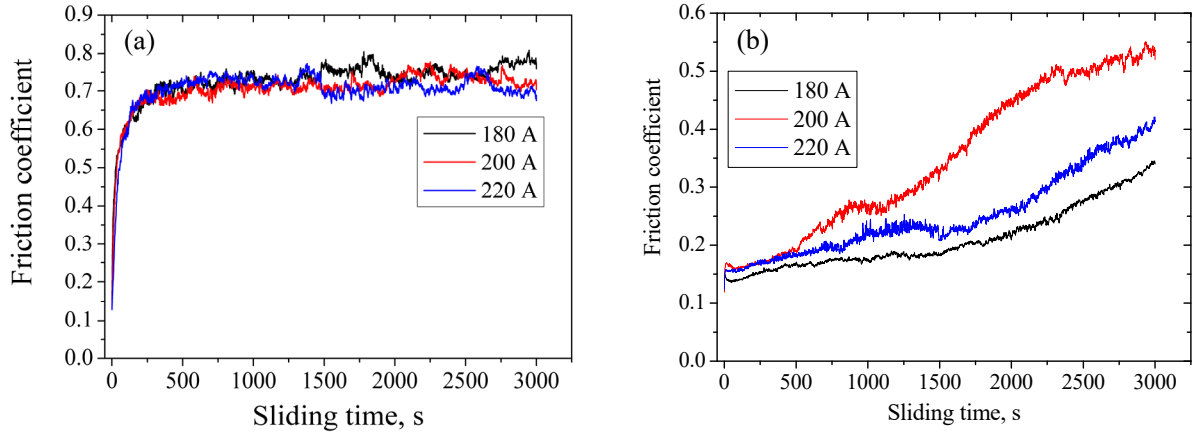

Figure 6. Dependence of the friction coefficient on the sliding time for (**a**) Al_2O_3 and (**b**) Al_2O_3-graphite coatings.

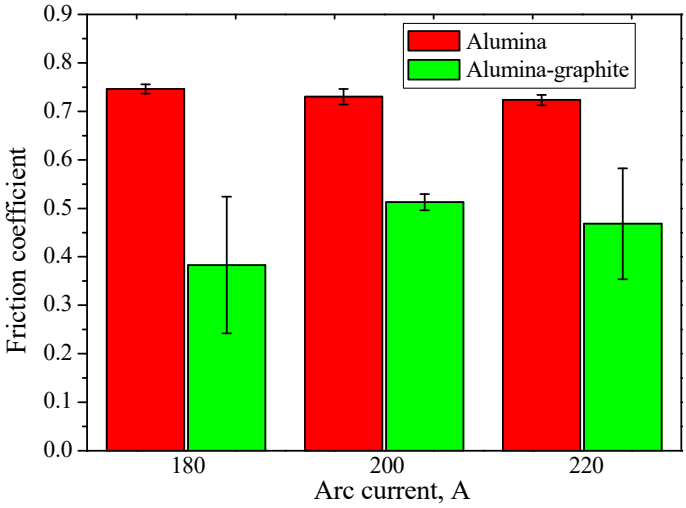

Figure 7. Average friction coefficient of the alumina and alumina-graphite coatings.

With the increase in arc current from 180 A to 220 A, the plasma temperature increases by 100 K, and therefore, the Al_2O_3 particles will be melted more. The surface morphology of the Al_2O_3 coatings also demonstrated that at higher torch powers, a more compact morphology was obtained. Thus, better contact between individual splats was formed. It could also reduce the level of micropore volume typically obtained at the splat boundaries of the sprayed A_2O_3 coatings [10,15,43]. The results demonstrated that the tribological properties of Al_2O_3 were slightly improved with the increase in arc current due to better contact between splats and the reduced number of pores at splat boundaries. The marginal increase in the γ-Al_2O_3 content in the coatings also demonstrates an increased melting degree of the feedstock particles and, therefore, better adhesion [15,22]. Thus, the wear debris produced during the tribological test would be lower at higher arc currents due to the improved adhesive wear resistance of the coatings. As a result, a slight reduction of the friction coefficients (from 0.746 to 0.72) and the wear rates (from 4.55×10^{-5} to 3.88×10^{-5} $mm^3/(Nm)$) for the Al_2O_3 coatings were observed.

In the case of alumina-graphite coatings (Figure 6b), there was rather a wavy trend, with the overall friction coefficient first increasing from 180 A to 200 A and then decreasing from 200 to 220 A. The friction coefficient of the AG1 coating was 0.134 after 250 s and gradually increased to 0.34 at the end of the sliding distance. The fastest rise in friction coefficient was recorded when the arc current was set at 200 A. The friction coefficient increased from 0.12 at the beginning of the test to 0.52 at the end. Meanwhile, the friction coefficient of the AG3 coating demonstrated a gradual increase along the entire sliding test ranking from 0.15 (at 250 s) to 0.421 (at the end of the test) (Figure 6b). The reduced friction coefficient values are related to the presence of graphite particles in the Al_2O_3-graphite coatings, which act as self-lubricants during dry sliding [34,38,43]. The increase in graphite concentration in the Ni-Al_2O_3 coatings reduced the wear rate [38]. However, if the graphite content reached critical values, the microhardness decreased due to increased defects and caused further severe wear.

As regards the average friction coefficient for alumina (Figure 7), with a load of 0.8 N, it was noted that the coefficient of friction varied from 0.746, 0.730 to 0.723 with an increase in torch power, respectively. With the addition of graphite, the reduction of friction coefficient in the range of 2700–3000 s was quite sharp, from 0.746 to 0.383, from 0.730 to 0.513, and from 0.723 to 0.468 for arc currents of 180, 200, and 220 A, respectively. However, within alumina-graphite coatings, the trend of friction coefficient was non-uniform, with an initial increase in friction coefficient and then a decrease with the increase in torch power.

With regard to the normalized wear rate (Figure 8), the variation for alumina coatings had a decreasing trend from 4.55×10^{-5}, 3.97×10^{-5} mm^3/Nm to 3.88×10^{-5} mm^3/Nm. Meanwhile, the trend in the wear rate of the alumina-graphite coatings was non-linear. With the increase in torch power, there was an initial increase in wear rate from 5.47×10^{-5} to 6.49×10^{-5} mm^3/Nm and then a drop to 2.41×10^{-5} mm^3/Nm was observed. These results demonstrated that by changing the torch power, it is possible to reduce the specific wear rate of the alumina-graphite coatings more than two times. It should be noted that the alumina-graphite coatings deposited at the highest torch power demonstrated the lowest wear rate values.

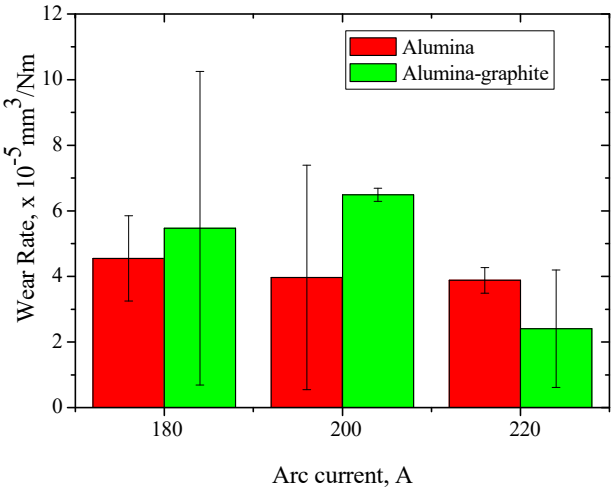

Figure 8. Normalized wear rate of the alumina and alumina-graphite coatings.

SEM morphologies of the worn surfaces of Al_2O_3 and Al_2O_3-graphite coatings sprayed at various torch powers are shown in Figure 9. The wear scars on the Al_2O_3 surface are not a continuous path (Figure 9a,b). The wear path of Al_2O_3 is relatively smooth; there is no evidence of grooving or the appearance of cracks. However, small microparticles could be found on the surface. The appearance of the Al_2O_3 particles is attributed to the brittle fracture of the Al_2O_3 coatings by stress cycling in the tribological sliding tests. It was demonstrated that abrasive wear and detachment are the main reasons for wear damage to the ceramic coatings [32,34,36,43–45]. Figure 9 c and d show the surface of the Al_2O_3-graphite coatings after sliding against an Al_2O_3 ball. The existence of the micro-cracks was obtained on the Al_2O_3-graphite coatings after a dry sliding test (Figure 9c,d). The increase in torch power slightly reduced the number of microcracks.

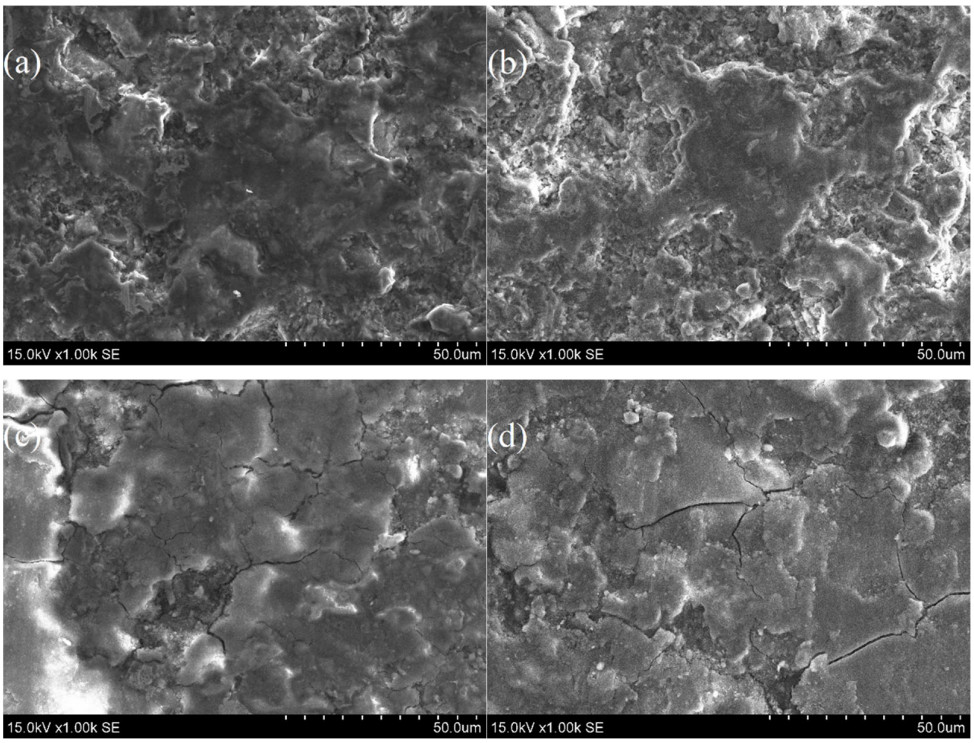

Figure 9. SEM images of the worn surface of the (**a**,**b**) Al_2O_3 and (**c**,**d**) Al_2O_3-graphite coatings deposited at the (**a**,**c**) lowest and the (**b**,**d**) highest torch powers.

It was observed that the formation of a self-lubricating graphite layer in the contact zone between the coatings and counterbody materials decreases the friction coefficient and could reduce the wear rate of the composites or composite coatings [36–38,46–49]. However, the addition of softer materials (e.g., graphite) in ceramic coatings, especially in high concentrations, reduces their hardness, fracture toughness, and cohesion values between the individual splats. In some cases, the composites or coatings with a relatively high fraction of graphite demonstrate a gradual increase in friction coefficient versus sliding time (distance) [36–38,45,48]. The coefficient of friction begins to increase because, during the friction, the graphite layer is constantly destroyed due to the debris of hard aluminum oxide particles appearing in the sliding zone. The detached alumina particles serve as an abrasive material and induce damage to the self-lubricating graphite layer [32–34,44]. The increase of the friction coefficient versus sliding time leads to the suggestion that the amount of alumina particles and debris removed from the surface of coatings during the sliding tests was enhanced and promoted faster disintegration of the formed graphite layer. Thus, as the friction process continues, the graphite layer is increasingly destroyed, which leads to a higher friction coefficient and enhances the wear rate of coatings.

The melting degree of the feedstock particles was enhanced, and generally, the mechanical properties of the coatings increased with the increase in torch power. However, in the case of plasma-sprayed alumina-graphite coatings, it is hard to expect an increase in fracture toughness and hardness due to the high amount of graphite. Also, the concentration of the graphite for the coating deposited at the highest torch power was slightly reduced (from 30 wt.% to 26 wt.%) due to increased sublimation of the graphite at higher temperatures. As a result, the friction coefficient of the AG3 coating was higher compared to the AG1 coating (Fig.7).

The properties of alumina coatings with an increase in torch power had friction coefficients and wear rates that were directly related to each other. This could be related to the improvement in the compactness and melting degree of the coating with increasing torch

power [34,43]. Thus, the property of the alumina coating deposited at 42 kW was found to be superior. This also has connections with the stable oxidative properties of the alumina coatings, which were quite similar and substantially pronounced for the coating at the highest torch power from the O/Al ratio. The α-Al_2O_3 and γ-Al_2O_3 phases furthermore contributed to the improvement in the microhardness and the wear-resistant properties of the coatings [36,42]. With reference to the alumina-graphite coatings, with the decrease in torch power from ~42 down to ~36 kW, the friction coefficient decreased initially, which is related to the increased carbon wt.% formation, and it being a soft material caused interfacial delamination during friction runs, further causing third-body abrasive wear. Though graphite/carbon composites have excellent strength, elevated thermal conductivity, and neat thermal shock resistance [50], the optimum residual carbon weight percentage is crucial [51]. This implies that above a certain limit of carbon, the effect of lubrication could be superseded by delamination and poor wear resistance [32,36]. It was also shown that another plasma spraying parameter, such as spraying distance, influenced the residual graphite weight percentage and even led to the transformation of the morphology. This had a direct effect on the mechanical and tribological properties [52]. A dense structure was formed in the case with the highest torch power at 42 kW, with substantial and possible re-graphitization. Excellent wear resistance and high microhardness were reported for a case with fine flake graphite with a dense structure and re-graphitization properties [38,53]. It was also shown that, owing to the mismatches in the thermal expansion, a feasible energy condition had to be derived to achieve a well-bonded, strain-free, and homogeneous coating, eliminating crack formations [54,55]. At mid-torch power (200 A), there could be a cessation of the graphitic film, leading to sub-metallic contact tribology, leading to the highest wear rate and highest friction coefficient [55]. With the lowest torch power (180 A), there could have been the optimum carbon wt.% in play, leading to the lowest friction coefficient and mid-level wear. At the highest torch power (42 kW), re-graphitization could have aided in the mid-level friction coefficient and the lowest wear rate.

4. Conclusions

Al_2O_3 and Al_2O_3-graphite coatings were formed by plasma spraying. The increase in torch power increased the mean plasma temperature by ~100 K and the surface roughness of the as-sprayed coatings. However, the incorporation of graphite in the feedstock powders reduced the surface roughness of Al_2O_3-graphite coatings down to 25%. It should be noted that the amount of graphite in the as-sprayed coatings was up to 3 times higher, compared to feedstock powders. The carbon content in the coatings was reduced from ~30 wt.% to ~26 wt.% with the increase in arc current from 180 A to 220 A. The friction coefficient of Al_2O_3 coatings slightly decreased from 0.746 to 0.723 as the wear rate reduced from 4.55×10^{-5} to 3.88×10^{-5} mm^3/Nm with the increase in torch power. The alumina-graphite composite coatings exhibited self-lubricating behavior under dry sliding conditions. The presence of graphite reduced the friction coefficient of Al_2O_3-graphite coatings. It was demonstrated that the friction coefficients of alumina-graphite coatings were lower by 30%–49% at the end of dry-sliding tests (at a sliding time range of 2700–3000 s) compared to alumina coatings without the significant enhancement of wear rate. The lowest wear rates were obtained for the coatings sprayed at the highest torch power due to the highest melting degree of particles, which increased the bonding contact between individual splats. The performed investigations indicated that the alumina-graphite coatings demonstrated lower friction coefficient values when the sliding distance was up to 150 m. The future work would be to evaluate the friction coefficient trend at higher sliding distances and determine the optimal graphite concentration in the alumina coatings.

Author Contributions: Conceptualization, J.S.M.; R.K. and L.M.; methodology, J.S.M. and L.M.; software, J.S.M. and R.K.; validation, J.S.M.; M.K. and Ž.K.; formal analysis, J.S.M.; M.K and L.M.; investigation, J.S.M.; M.K.; R.K.; Ž.K. and L.M.; resources, R.K. and L.M.; data curation, J.S.M.; writ-

ing—original draft preparation, J.S.M. and L.M.; writing—review and editing, J.S.M. and L.M.; visualization, Ž.K.; J.S.M. and L.M.; supervision, J.S.M.; project administration, L.M.; funding acquisition, L.M. All authors have read and agreed to the published version of the manuscript.

Funding: This research received no external funding.

Institutional Review Board Statement: Not applicable.

Informed Consent Statement: Not applicable.

Data Availability Statement: Not applicable.

Conflicts of Interest: The authors declare no conflicts of interest.

References

1. Jambagi, S.C.; Kar, S.; Brodard, P.; Bandyopadhyay, P.P. Characteristics of plasma sprayed coatings produced from carbon nanotube doped ceramic powder feedstock. *Mater. Des.* **2016**, *112*, 392–401.
2. Kim, K.H.; Kim, J.H.; Hong, K.W.; Park, J.Y.; Lee, C.B. Application of high-temperature ceramic plasma-spray coatings for a reusable melting crucible. *Surf. Coatings Technol.* **2017**, *326*, 429–435.
3. Liu, Z.; Xing, Z.; Wang, H.; Xue, Z.; Chen, S.; Jin, G.; Cui, X. Effect of ZnO on the microstructure and dielectric properties of BaTiO3 ceramic coatings prepared by plasma spraying. *J. Alloys Compd.* **2017**, *727*, 696–705.
4. Li, G.R.; Yang, G.J.; Li, C.X.; Li, C.J. Force transmission and its effect on structural changes in plasma-sprayed lamellar ceramic coatings. *J. Eur. Ceram. Soc.* **2017**, *37*, 2877–2888.
5. Deng, W.; Li, S.; Liu, X.; Zhao, X.; An, Y.; Zhou, H.; Chen, J. A novel approach to fabricate hybrid materials with excellent tribological properties from spray-formed ceramic. *Mater. Lett.* **2017**, *193*, 199–202.
6. Tlili, B.; Barkaoui, A.; Walock, M. Tribology and wear resistance of the stainless steel. The sol–gel coating impact on the friction and damage. *Tribol. Int.* **2016**, *102*, 348–354.
7. Holmberg, K.; Laukkanen, A.; Ghabchi, A.; Rombouts, M.; Turunen, E.; Waudby, R.; Suhonen, T.; Valtonen, K.; Sarlin, E. Computational modelling based wear resistance analysis of thick composite coatings. *Tribol. Int.* **2014,** *72*, 13–30.
8. Heimann, R.B. *Plasma Spray Coating Principles and Applications*; Wiley-VCH: Hoboken, NJ, USA, 2008.
9. Fauchais, M.B. P. L.; Heberlein, J.V.R. Thermal Spray Fundamentals. In *From Powder to Part*; Springer: Berlin/Heidelberg, Germany, 2014**.**
10. Yang, Y.; Wang, Y.; Tian, W.; Yan, D.; Zhang, J.; Wang, L. Influence of composite powders' microstructure on the microstructure and properties of Al_2O_3–TiO_2 coatings fabricated by plasma spraying. *Mater. Des.* **2015**, *65*, 814–822.
11. Song, E.P.; Hwang, B.; Lee, S.; Kim, N.J.; Ahn, J. Correlation of microstructure with hardness and wear resistance of stainless steel blend coatings fabricated by atmospheric plasma spraying. *Mater. Sci. Eng. A.* **2006**, *429*, 189–195.
12. Lin, X.; Zeng, Y.; Ding, C.; Zhang, P. Effects of temperature on tribological properties of nanostructured and conventional Al2O3–3 wt.% TiO_2 coatings. *Wear* **2004**, *256*, 1018–1025.
13. Yin, Z.; Tao, S.; Zhou, X.; Ding, C. Particle in-flight behavior and its influence on the microstructure and mechanical properties of plasma-sprayed Al_2O_3 coatings. *J. Eur. Ceram. Soc.* **2008**, *28*, 1143–1148.
14. Sahab, A.R.M.; Saad, N.H.; Kasolang, S.; Saedon, J. Impact of Plasma Spray Variables Parameters on Mechanical and Wear Behaviour of Plasma Sprayed Al_2O_3 3%wt TiO_2 *Coat. Abrasion Eros. Appl. Procedia Eng*. **2012**, *41*, 1689–1695.
15. Wang, C.; Fan, L.; Fan, J.; Zhang, D.; Wang, H. Effect of spraying power on microstructure and properties of supersonic plasma sprayed Al_2O_3 coating on porous Si_3N_4 substrate. *J. Alloys Compd.* **2013**, *559*, 152–157.
16. Song, E.P.; Ahn, J.; Lee, S.; Kim, N.J. Effects of critical plasma spray parameter and spray distance on wear resistance of Al_2O_3–8 wt.%TiO_2 coatings plasma-sprayed with nanopowders. *Surf. Coatings Technol.* **2008**, *202*, 3625–3632.
17. Shahien, M.; Suzuki, M. Low power consumption suspension plasma spray system for ceramic coating deposition. *Surf. Coatings Technol.* **2017**, *318*, 11–17.
18. Jambagi, S.C. Scratch adhesion strength of plasma sprayed carbon nanotube reinforced ceramic coatings. *J. Alloys Compd.* **2017**, *728*, 126–137.
19. Wang, R.; Song, D.; Liu, W. Effect of arc spraying power on the microstructure and mechanical properties of Pb-Sn coating deposited onto carbon fiber reinforced epoxy composites. *Polym. Polym. Compos.* **2011**, *19*, 289–294.
20. Wu, H.; Li, H.J.; Lei, Q.; Fu, Q.G.; Ma, C.; Yao, D.J.; Wang. Y. J.; Sun, C.; Wei, J.F.; Han, Z.H. Effect of spraying power on microstructure and bonding strength of MoSi2-based coatings prepared by supersonic plasma spraying. *Appl. Surf. Sci.* **2011**, *257*, 5566–5570.
21. Wang, J.; Sun, J.; Zhang, H.; Dong, S.; Jiang, J.; Deng, L.; Zhou, X.; Cao, X. Effect of spraying power on microstructure and property of nanostructured YSZ thermal barrier coatings. *J. Alloys Compd.* **2018**, *730*, 471–482.
22. Wang, C.; Li, K.; Shi, X.; Huo, C.; He, Q.; Zhang, Y. Effect of spraying power on oxidation resistance and mechanical properties of plasma sprayed La-Mo-Si coating. *Surf. Coatings Technol.* **2017**, *311*, 138–150.
23. Zhang, X.C.; Xu, B.S.; Tu, S.T.; Xuan, F.Z.; Wang, H.D.; Wu, Y.X. Effect of spraying power on the microstructure and mechanical properties of supersonic plasma-sprayed Ni-based alloy coatings. *Appl. Surf. Sci.* **2008**, *254*, 6318–6326.

24. Xing, Y.Z.; Liu, Z.; Wang, G.; Li, X.H.; Xing, Y.L.; Jiang, C.P.; Chen, Y.N.; Song, X.; Dargusch, D.M. Effects of spray parameters on the adhesion between plasma-sprayed cast iron splat and aluminium substrate. *Surf. Coatings Technol.* **2017**, *315*, 1–8.
25. Zhao, D.; Coyle, T.W.; Chien, K. Phase composition and microstructure of yttrium aluminum garnet (YAG) coatings prepared by suspension plasma spraying of Y_2O_3-Al_2O_3 powders. *Surf. Coatings Technol.* **2013**, *235*, 303–309.
26. Sivakumar, G.; Dusane, R.O.; Joshi, S.V. A novel approach to process phase pure α-Al_2O_3 coatings by solution precursor plasma spraying. *J. Eur. Ceram. Soc.* **2013**, *33*, 2823–2829.
27. Song, R.G.; Wang, C.; Jiang, Y.; Li, G.; Lu, H.; Wang, Z.X. Microstructure and properties of Al_2O_3/TiO_2 nanostructured ceramic composite coatings prepared by plasma spraying. *J. Alloys Compd.* **2012**, *544*, 13–18.
28. Li, C.J.; Sun, B. Effects of spray parameters on the microstructure and property of Al_2O_3 coatings sprayed by a low power plasma torch with a novel hollow cathode. *Thin Solid Films.* **2004**, *450*, 282–289.
29. Gao, Y.; Xu, X.; Yan, Z.; Xin, G. High hardness alumina coatings prepared by low power plasma spraying. *Surf. Coatings Technol.* **2002**, *154*, 189–193.
30. Bu, Z.; Zhao, X.; Liu, Xue, Y.; An, Y. Effect of Melting Behavior of Al_2O_3 Powder on the Structure and Dielectric Properties of Plasma-Sprayed Coatings. *J. Therm. Spray Tech.* **2022**, 31, 449–461.
31. Bolelli, G.; Cannillo, V.; Lusvarghi, L.; Manfredini, T. Wear behaviour of thermally sprayed ceramic oxide coatings, Wear. **2006**, *261*, 1298–1315. https://doi.org/10.1016/j.wear.2006.03.023.
32. Mahade, S.; Mulone, A.; Bjorklund, S.; Klement, U.; Joshi, S. Incorporation of graphene nano platelets in suspension plasma sprayed alumina coatings for improved tribological properties. *Appl. Surf. Sci.* **2021**, *570*, 151227.
33. Liu, C.; Sun, J.; Venturi, F.; Romero, A.; Hussain, T. Microstructure and wear performance of alumina/graphene coating on textured Al_2O_3/TiC substrate composites. *J. Eur. Ceram.* **2021**, *41*, 1438–1451.
34. Li, Y.; Liu, J.; Deng, J.; He, J.; Qin, Y.; Xing, Y.; Yin. F. Fabrication of graphene oxide reinforced plasma sprayed Al_2O_3 coatings. *Ceram. Int.* **2023**, *49*, 1667–1677.
35. Marcinauskas, L.; Mathew, J.S.; Milieška, M.; Aikas, M.; Kalin. M. Influence of graphite content on the tribological properties of plasma sprayed alumina-graphite coatings. *Surf. Interfaces* **2023**, *38*, 102763.
36. Marcinauskas, L.; Mathew, J.S.; Milieška, M.; Thanigachalam, B.; Kupec, A.; Česnavičius, R.; Kėželis, R.; Kalin, M. Microstructure and tribological properties of plasma sprayed alumina and alumina-graphite coatings. *Surf. Coat. Technol.* **2018**, *350*, 401–409.
37. Marcinauskas, L.; Mathew, J.S.; Milieška, M.; Aikas, M.; Kalin. M. Effect of graphite concentration on the tribological performance of alumina coatings. *J. Alloys Compd.* **2020**, *827*, 154135.
38. Zhao, X.; Li, S.; Hou, G.; An, Y.; Zhou, H.; Chen, J. Influence of doping graphite on microstructure and tribological properties of plasma sprayed $3Al_2O_3$-$2SiO_2$ coating. *Tribol. Int.* **2016**, *101*, 168–177.
39. Brinkienė, K.; Kėželis, R.; Mečius, V. Effect of outlet nozzle design on the YSZ particle in-flight characteristics in plasma jet generated by DC plasma torch. *In Advances in Heat Transfer Engineering; Begell House: Danbury, CT, USA, 2003; pp. 629–636.*
40. Marcinauskas, L.; Milieška, M.; Kėželis, R. Effect of torch power on the microstructure of plasma sprayed Al_2O_3 coatings. *Surf. Interface Anal.* **2016**, *48*, 552–555.
41. Marcinauskas, L.; Kavaliauskas, Ž.; Kėželis, R. Formation of carbon composite coatings by plasma spraying. *Vacuum* **2015**, *122*, 326–331.
42. Kim, J.T.; Lim, K.B.; Lee, D.C. Fabrication of alumina films as a thermoelectric material by thermal plasma processing. *Surf. Interface Anal.* **2003**, *35*, 658–661.
43. Ghara, T.; Bandyopadhyay, P. Understanding the role of in-flight particle temperature and velocity on the residual stress depth profile and other mechanical properties of atmospheric plasma sprayed Al_2O_3 coating. *J. Eur. Ceram*. **2022**, *42*, 4353–4368.
44. Pattnayak, A.; Gupta, N.V.; Abhijith, D.; Kumar, J.; Jain, V. Chaudhry. Development of rGO doped alumina-based wear and corrosion resistant ceramic coatings on steel using HVOF thermal spray. *Ceram. Int.* **2023**, *49*, 17577–17591.
45. Mu, M.; Zhou, X.; Xiao, Q.; Liang, J.; Huo, X. Preparation and tribological properties of self-lubricating TiO_2/graphite composite coating on Ti_6Al_4V alloy. *Appl. Surf. Sci.* **2021**, *258*, 8570–8576.
46. Ordonez, M.F.C.; Farias, M.C.M.; Descartes, S.; Machado, I.F.; Souza, R.M. Tribofilm formation during dry sliding of graphite- and MoS2- based composites obtained by spark plasma sintering. *Tribol. Int.* **2021**, *160*, 107035.
47. Murakami, T.; Matsuzaki, K.; Inui, H. Microstructure, friction and wear properties of αFeSi 2–graphite composite specimens. *Tribol. Int.* **2013**, *67*, 98–103.
48. Hou, B.; Guo, H.; Zhang, N.; Zhi, Q.; Yang, J. Anisotropic Friction Derived from the Layered Arrangement of the Oriented Graphite Flakes in the Copper–Iron Matrix Composite. *Tribol. Lett*. **2022**, *78*, 1–13.
49. Torres, H.; Podgornik, B.; Klug, M.; Ripol, M. Compatibility of graphite, hBN and graphene with self-lubricating coatings and tool steel for high temperature aluminium forming. Wear 2022, 204187.
50. Kim, H.; Oh, P.Y.; Kang, B.R.; Lim, H.; Moon, M.; Hong, B.G. Ablation properties of plasma facing materials using thermal plasmas. *Fusion Eng. Des.* **2017**, *124*, 460–463.
51. Shiby; M. J.; Marcinauskas, L.; Thanigachalam, B.; Česnavičius, R.; Milieška, M.; Kėželis, R.; Kupec, A..; Kalin, M. The tribological properties of Al_2O_3 based composite coatings deposited by plasma spraying, *in: CYSENI 2018 15th Int. Conf. Young Sci. Energy* 2018, 425–434.
52. Qin, Y.; Zhu, L.; He, J.; Yin, F.; Nan, Z. Effect of powder injection distance on microstructure and mechanical properties of reactive plasma sprayed TiCN coatings. *Surf. Coatings Technol.* **2017**, *329*, 131–138.

53. Qin, Y.; He, J.; Yin, F.; Liu, B.; Zhang, F. Effect of Ti particle size on mechanical and tribological properties of TiCN coatings prepared by reactive plasma spraying. *Ceram. Int.* **2017**, *43*, 16548–16554.
54. 543 Robotti, M.; Dosta, S.; Gardon, M.; Cano, I.G.; Guilemany, J.M.; Kourasi, M.; Mellor, B.; Wills, R. Enhancing the performance of common electrode materials by means of atmospheric plasma spray coatings. *J. Energy Storage.* **2016**, *5*, 127–133.
55. Huang, C.; Li, W.; Planche, M.P.; Liao, H.; Montavon, G. In-situ formation of Ni-Al intermetallics-coated graphite/Al composite in a cold-sprayed coating and its high temperature tribological behaviors. *J. Mater. Sci. Technol.* **2017**, *33*, 507–515.